M$_2$(*m*-dobdc) (M = Mg, Mn, Fe, Co, Ni) Metal−Organic Frameworks Exhibiting Increased Charge Density and Enhanced H$_2$ Binding at the Open Metal Sites

Matthew T. Kapelewski,[†] Stephen J. Geier,[†,¶] Matthew R. Hudson,[‡] David Stück,[†] Jarad A. Mason,[†] Jocienne N. Nelson,[§] Dianne J. Xiao,[†] Zeric Hulvey,[‡,∥] Elizabeth Gilmour,[§] Stephen A. FitzGerald,[§] Martin Head-Gordon,[†,⊥] Craig M. Brown,[‡,#] and Jeffrey R. Long*[,†,∇]

[†]Department of Chemistry, University of California, Berkeley, Berkeley, California 94720, United States

[‡]Center for Neutron Research, National Institute of Standards and Technology, Gaithersburg, Maryland 20899, United States

[§]Department of Physics, Oberlin College, Oberlin, Ohio 44074, United States

[∥]Department of Materials Science and Engineering, University of Maryland, College Park, Maryland 20742, United States

[⊥]Chemical Sciences Division and [∇]Materials Sciences Division, Lawrence Berkeley National Laboratory, Berkeley, California 94720, United States

[#]Chemical and Biomolecular Engineering, University of Delaware, Newark, Delaware 19716, United States

Ⓢ *Supporting Information*

ABSTRACT: The well-known frameworks of the type M$_2$(dobdc) (dobdc^{4-} = 2,5-dioxido-1,4-benzenedicarboxylate) have numerous potential applications in gas storage and separations, owing to their exceptionally high concentration of coordinatively unsaturated metal surface sites, which can interact strongly with small gas molecules such as H$_2$. Employing a related meta-functionalized linker that is readily obtained from resorcinol, we now report a family of structural isomers of this framework, M$_2$(*m*-dobdc) (M = Mg, Mn, Fe, Co, Ni; *m*-dobdc^{4-} = 4,6-dioxido-1,3-benzenedicarboxylate), featuring exposed M^{2+} cation sites with a higher apparent charge density. The regioisomeric linker alters the symmetry of the ligand field at the metal sites, leading to increases of 0.4−1.5 kJ/mol in the H$_2$ binding enthalpies relative to M$_2$(dobdc). A variety of techniques, including powder X-ray and neutron diffraction, inelastic neutron scattering, infrared spectroscopy, and first-principles electronic structure calculations, are applied in elucidating how these subtle structural and electronic differences give rise to such increases. Importantly, similar enhancements can be anticipated for the gas storage and separation properties of this new family of robust and potentially inexpensive metal−organic frameworks.
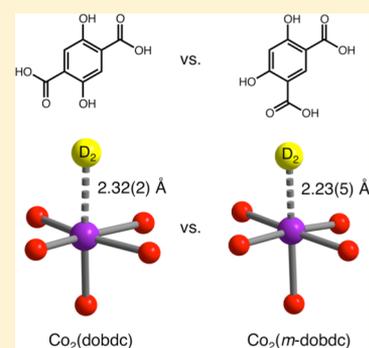
INTRODUCTION

Metal−organic frameworks are a well-known class of porous materials comprised of inorganic units bridged by coordinating organic linkers. In addition to possessing high internal surface areas, their physical and chemical properties can be tuned for specific applications by judicious choice of the metal center and organic ligand. These properties lead to applications in storing and separating gases, in which it is particularly important to have precise control over the strength and specificity of interactions between the pore surface and various potential adsorbates.[1] Indeed, strong adsorption sites are often installed on the pore surface in order to attract specific gas molecules selectively for separation applications or to increase the density of gas molecules present for storage applications.[1h,j,2]

Exposed metal cations represent an important example of strong adsorption sites that have been realized in many metal−organic frameworks.[3] These Lewis acidic sites, which are typically formed by removing metal-coordinated solvent molecules upon heating under reduced pressure, are highly polarizing and have strong interactions with many small gas molecules.[3a,4] For example, the well-established M$_2$(dobdc) (M = Mg, Mn, Fe, Co, Ni, Cu, Zn; dobdc^{4-} = 2,5-dioxido-1,4-benzenedicarboxylate) structure type, also known as M-MOF-74, CPO-27-M, or M$_2$(dhtp),[5] contains a high density of exposed metal cations and is especially promising for the storage of a wide variety of gases. As a result of its compact, highly charged tetraanionic linker, this framework is endowed with an exceptionally high density of open metal coordination sites, which are the primary binding sites for small gas molecules such as H$_2$, CH$_4$, C$_2$H$_4$, and CO$_2$. Consequently, M$_2$(dobdc) frameworks have been investigated for numerous potential applications involving gas adsorption, including H$_2$ storage,[3a,4a,c,6] methane storage,[4b,7] CO$_2$ capture,[8] and hydrocarbon separations.[1i,9] All of these applications take advantage

of strong interactions between gas molecules and exposed metal cations.

Discovering new frameworks with a high density of open metal coordination sites is not trivial, as it is difficult to predict what topologies will form with partial solvation of the metal nodes and will then further be amenable to desolvation. Rather, selectively tuning the most promising of the numerous existing frameworks by altering the linker, the metal, or both provides a viable strategy for developing promising new adsorbents. Since the M_2(dobdc) series of frameworks has high chemical and thermal stability[8b,10] and has been shown to be outstanding for binding a high capacity of small gas molecules, we hoped to modify this framework by tuning the electronics of the exposed metal cations, which should subsequently tune the affinity for different gas molecules. For example, the binding of H_2 or CH_4 might be enhanced by increasing the positive charge density at the metal cation site, thus increasing its ability to polarize and bind adsorbing gas molecules more strongly. Furthermore, M_2(dobdc) offers the advantage of being an isostructural series of frameworks that can be formed with a variety of metals, thereby offering an additional level of control for tuning the framework for specific interactions. Based on the high density of exposed metal cations, isostructural nature of the these frameworks, and thermal stability, a combination of properties that is not paralleled by any other structure type, M_2(dobdc) provides an ideal platform for exploring the tunability of metal−organic frameworks to strengthen framework−gas interactions.

This work outlines the synthesis of a structural isomer of the M_2(dobdc) framework, which will be referred to as M_2(m-dobdc) (m-dobdc^{4-} = 4,6-dioxido-1,3-benzenedicarboxylate). Rather than having *para* carboxylic acid functionalities and *para* hydroxyl substituents, as in the regular H_4dobdc linker, H_4(m-dobdc) has *meta* carboxylic acid groups and *meta* hydroxyl substituents. The H_4(m-dobdc) linker was targeted due to its ease of synthesis and potentially low cost. Indeed, a solvent-free Kolbe−Schmitt reaction to produce H_4(m-dobdc) using only resorcinol, $KHCO_3$, and CO_2 is efficient and inexpensive. In spite of this linker isomerism, it is still possible to form a framework with a similar overall structure, replete with one-dimensional hexagonal channels and a high density of open metal coordination sites. This structural isomerism takes advantage of the fact that M_2(dobdc) frameworks have multiple types of coordinating functional groups in the linker, which is a rarity among most well-known metal−organic frameworks.

The resulting new framework has subtle differences in the electronic structure of the ligand and overall connectivity as compared to the M_2(dobdc) framework, which might be expected to influence interactions with small gas molecules by changing the local environment around the open metal coordination sites. Isomers of metal−organic frameworks are known and primarily derive from what are termed "framework isomers." The structure of M_2(m-dobdc), however, is an example of a ligand-originated isomer.[11] Relatedly, a recent M_2(dobdc) analogue was synthesized with thiols rather than phenols,[12] but a purely structural isomer of M_2(dobdc) has never before been synthesized.

Here, H_2 adsorption is used as a probe to determine whether this new framework exhibits enhanced gas adsorption properties. The choice of H_2 as a probe molecule originates from its simplicity, low polarizability, and potential use as a clean, renewable fuel.[2a,13] Through the use of H_2 adsorption isotherms, powder neutron diffraction, inelastic neutron scattering, infrared spectroscopy, and first-principles electronic structure calculations, we provide a careful comparison of the differences between M_2(dobdc) and M_2(m-dobdc) that contribute to the differences in their H_2 adsorption properties.

■ EXPERIMENTAL SECTION

Methanol was purchased from commercial vendors, further dried over molecular sieves, and deoxygenated by purging with N_2. All other reagents were purchased from commercial vendors and used without further purification, unless otherwise noted. The H_4(m-dobdc) ligand was synthesized according to a literature procedure.[14]

Synthesis of M_2(m-dobdc) (M = Mn, Fe, Co, Ni). Anhydrous MCl_2 (3.0 mmol) and H_4(m-dobdc) (240 mg, 1.2 mmol) were added to 80 mL of a mixed solvent (x% MeOH by volume in dimethylformamide (DMF), where for Mn, x = 15; Fe, x = 15; Co, x = 50; Ni, x = 35) in a nitrogen-filled glovebox for M = Mn, Fe and in air for M = Co, Ni. The solution was dispensed into eight 20 mL scintillation vials, which were each sealed with a PTFE-lined cap and heated at 120 °C for 18 h. The resulting solid from each vial was combined, submerged in 20 mL of DMF, and heated at 70 °C for 24 h. The DMF was decanted and replaced with 20 mL of methanol. The resulting suspension was heated at 70 °C for 4 days, during which time the methanol was replaced every 24 h. The material was activated by heating it at 150 °C under dynamic vacuum on a Schlenk line for 12 h, followed by further activation of a small amount of the sample by heating the solid under dynamic vacuum (<10 μbar) at 180 °C (160 °C for Fe_2(m-dobdc)) for 24 h at a ramp rate of 0.5 °C/min. It should be noted that larger scale syntheses of Co_2(m-dobdc) and Ni_2(m-dobdc) were also accomplished with no loss in crystallinity or surface area by stirring at room temperature in a round-bottom flask equipped with a reflux condenser at a concentration of 20.2 mmol H_4(m-dobdc) and 50.5 mmol MCl_2 (M = Co, Ni) in 1250 mL solvent. Times and temperatures were identical to the small-scale synthesis, but 200 mL of solvent was used for each exchange.

Synthesis of Mg_2(m-dobdc). This compound was synthesized in air in a round-bottom flask by adding 300 mg of $Mg(NO_3)_2 \cdot 6H_2O$ and 93 mg of H_4(m-dobdc) to 14 mL MeOH in 31 mL DMF and stirring at 120 °C for 8 h, then filtering off the resulting solid. Detailed characterization of all frameworks is contained in the Supporting Information.

Physical Measurements. Thermogravimetric analyses were carried out at a ramp rate of 2 °C/min under a 25 mL/min N_2 flow with a TA Instruments TGA Q5000. Infrared spectra were collected on a PerkinElmer Avance Spectrum 400 FTIR spectrometer equipped with a Pike attenuated total reflectance (ATR) accessory. Diffraction data were collected with 0.02° steps using a Bruker AXS D8 Advance diffractometer equipped with Cu−Kα radiation (λ = 1.5418 Å), a Göbel mirror, a Lynxeye linear position-sensitive director, and mounting the following optics: fixed divergence slit (0.6 mm), receiving slit (3 mm), and secondary beam Soller slits (2.5°). The generator was set at 40 kV and 40 mA. Samples were either loaded on zero background sample holders or packed into air-free capillaries in a nitrogen-filled glovebox and mounted using a capillary stage. Elemental analyses were obtained from the Microanalytical Laboratory of the University of California, Berkeley.

Gas Adsorption Measurements. Gas adsorption isotherms for pressures in the range 0−1.2 bar were measured using a volumetric method using either a Micromeritics ASAP2020 or ASAP2420 instrument. Samples were transferred under a dinitrogen atmosphere to preweighed analysis tubes, then capped with a Transeal. The samples were evacuated at elevated temperature until the outgas rate was <1 μbar/min, at which point the tube was weighed to determine the mass of the activated sample, which was typically 50−200 mg. The tube was transferred to the analysis port of the instrument and the outgas rate was again checked to ensure that it was <1 μbar/min. UHP-grade (99.999% purity) N_2, H_2, and He were used for all adsorption measurements. For all isotherms, warm and cold free spaces were measured using He; N_2 and H_2 isotherms at 77 and 87 K were measured in liquid nitrogen and liquid argon baths, respectively.

Oil-free vacuum pumps and oil-free pressure regulators were used for all measurements. Brunauer–Emmett–Teller (BET) and Langmuir surface areas were determined from N_2 adsorption data at 77 K using Micromeritics software.

Powder Neutron and X-ray Diffraction Experiments. Neutron powder diffraction (NPD) experiments were carried out on 0.8358, 0.9567, and 0.9702 g activated $Co_2(m\text{-dobdc})$, $Ni_2(m\text{-dobdc})$, and $Co_2(dobdc)$ samples respectively, using the high-resolution neutron powder diffractometer, BT1, at the National Institute of Standards and Technology Center for Neutron Research (NCNR). The samples were placed in a He purged glovebox and loaded into a vanadium sample can equipped with a valve for gas loading, and sealed using an indium O-ring. NPD data were collected using a Ge(311) monochromator with an in-pile 60′ collimator corresponding to a wavelength of 2.078 Å. The samples were loaded onto bottom-loading closed cycle refrigerators, and initial data collected on the activated $Co_2(m\text{-dobdc})$ and $Ni_2(m\text{-dobdc})$ frameworks at 10 K. As part of the initial structure solution, X-ray diffraction (XRD) measurements were carried out on 12.8 mg of $Co_2(m\text{-dobdc})$ at the Advanced Photon Source (APS) on the 17-BM materials diffractometer (λ = 0.7291 Å) at 298 K. The activated $Co_2(m\text{-dobdc})$ sample was transferred into quartz capillary in a He purged glovebox and wax sealed for the X-ray measurements. For comparison of the D_2 structural dependence on ligand connectivity, $Co_2(dobdc)$ and $Co_2(m\text{-dobdc})$ were each individually connected to a gas manifold of known volume and exposed to a known dose, approximately 0.75 and 2.25 D_2 per Co^{2+}, at 100 K (refined composition given in Tables S12–S14, S19). Both samples were slow cooled from 100 to 10 K to ensure full equilibration and complete adsorption, as evidenced by a zero pressure reading on the barometer by 25 K, for data collection. Further D_2 structural data were collected on $Co_2(m\text{-dobdc})$ and $Ni_2(m\text{-dobdc})$ as a function of dose with final loadings of 0.75, 1.25, 1.5, 1.75, 2.0, 2.25, and 3.0 D_2 per Co^{2+} and 1.0, 2.0, and 3.0 D_2 per Ni^{2+}. Structural data for H_2 were measured on $Co_2(m\text{-dobdc})$ at a loading of 0.7 H_2 per Co^{2+}. Refined compositions are given in Tables S12 and S15–S20 (Co) and Tables S21–S23 (Ni). Details on the structure solutions are available in the Supporting Information.

Inelastic Neutron Scattering. Inelastic neutron scattering (INS) spectra were collected using the Filter Analyzer Neutron Spectrometer (FANS)[15] at the NCNR on the same samples used for the NPD experiments. Spectra were obtained at 7 K using the pyrolytic graphite (002) monochromator and 20′-20′ collimation options. Data were first collected for the bare framework, followed by data collection for the sample loaded with *normal*-H_2 (*n*-H_2), which contains a 3:1 mixture of *ortho* (*o*-H_2) to *para* (*p*-H_2), respectively. For $Co_2(m\text{-dobdc})$, data were collected at loadings of 0.33, 0.5, 1.0, 2.0, 3.0, and 4.0 *n*-H_2 molecules per Co atom, while for $Ni_2(m\text{-dobdc})$ data were collected at loadings of 0.67, 1.0, 2.0, 3.0, and 4.0 *n*-H_2 molecules per Ni atom. Gas was loaded into the materials using the same methodology as described in the NPD experiments. The spectra of the bare frameworks were subtracted from the spectra obtained from the H_2 loaded samples, and Gaussian peaks were fit to the rotational transitions using the DAVE suite of programs.[16] Further measurements of the framework vibrational densities of states for the activated $Co_2(m\text{-dobdc})$ material were made to higher energies (35 to 160 meV) using the Cu(220) monochromator with 20′-20′ collimation.

Infrared Spectroscopy. Infrared spectra were acquired using a Bomem DA3Michelson interferometer equipped with a glowbar source, CaF_2 beamsplitter, and a liquid nitrogen cooled mercury–cadmium-telluride detector. A cutoff filter above 9000 cm^{-1} was used to prevent unwanted sample heating from the IR source. A custom-built diffuse reflectance system[17] with a sample chamber that allows both the temperature and atmosphere of the material to be controlled was used for all experiments. Powder samples of the frameworks (~10 mg) were transferred under inert atmosphere to a cup affixed to a copper slab providing thermal contact to a coldfinger cryostat (Janis ST-300T). The sample temperature was monitored by a Si-diode thermometer. Known quantities of H_2 gas were dispensed from a calibrated gas manifold by monitoring the change in pressure.

DFT Calculations. Due to the extended nature of the $M_2(dobdc)$ and $M_2(m\text{-dobdc})$ structures, cluster modeling was completed on the linker of interest coordinated to a pair of Co atoms bound to either end of the organic linker. To truncate the system, the ligating oxygen atoms that are not part of the included linker were added as formaldehyde molecules in order to conserve charge. The experimentally determined crystal structures were truncated as described and frozen. The geometry of a hydrogen molecule bound to the frozen system based on neutron diffraction data was then optimized. The range-separated, dispersion corrected functional ωB97X-D implemented in the electronic structure software Q-Chem[18] was used with an ultra fine (99, 590) grid and a triple split-valence basis set with polarization (6-311G**).[19] A small core Stuttgart–Born (SRSC) effective core potential is employed to model the core electrons of the Co.[20] Binding is further analyzed using the ALMO EDA.[21] Charge transfer is accounted for using the perturbative Roothaan step approach, which allows for assignment of forward and backbonding energies as well as generation of complementary occupied-virtual orbital pairs (COVPs)[22] to visualize charge transfer.

■ RESULTS AND DISCUSSION

Structural Characterization of $M_2(m\text{-dobdc})$. A less expensive regioisomer of H_4dobdc was selected in order to form a framework with the same overall topology and a high density of open sites as in $M_2(dobdc)$, but with potentially different local geometry and electronic properties. After the synthesis of $H_4(m\text{-dobdc})$ from resorcinol, it was possible to synthesize an isostructural series of $M_2(m\text{-dobdc})$ (M = Mg, Mn, Fe, Co, or Ni) frameworks (Figure 1) exhibiting powder
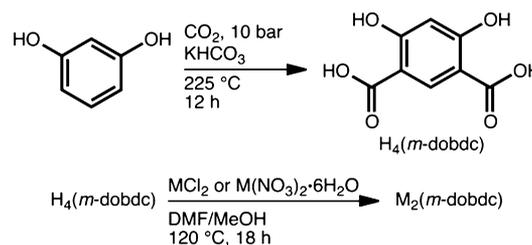
Figure 1. Synthesis of $H_4(m\text{-dobdc})$ and $M_2(m\text{-dobdc})$, starting from the inexpensive compound resorcinol.

X-ray diffraction patterns (Figures S1–S5) analogous to the respective $M_2(dobdc)$ frameworks, indicating that the two series adopt similar structures. Thermogravimetric analyses of the $Co_2(m\text{-dobdc})$ and $Ni_2(m\text{-dobdc})$ frameworks show initial mass losses of 33% and 14%, respectively, indicative of volatilization of trapped solvent molecules and thus porosity (Figure S6a). After repeatedly washing each compound with methanol to replace the metal-bound DMF, the frameworks were activated by heating under dynamic vacuum at 180 °C. Thermogravimetric analysis of the activated frameworks indicated that $Mn_2(m\text{-dobdc})$ and $Co_2(m\text{-dobdc})$ are stable to 250 °C and the $Ni_2(m\text{-dobdc})$ is stable to 350 °C.

To confirm that the $M_2(m\text{-dobdc})$ frameworks are indeed structurally analogous to $M_2(dobdc)$, powder X-ray and neutron diffraction experiments were used to solve the crystal structure of $Co_2(m\text{-dobdc})$ (Figure 2). Similar to $Co_2(dobdc)$, $Co_2(m\text{-dobdc})$ possesses helical chains of Co^{2+} centers running parallel to the crystallographic c axis. Upon activation and removal of a bound DMF molecule, each metal center is ligated by a combination of oxido and carboxylate donors in a square pyramidal geometry, with open coordination sites directed into the one-dimensional hexagonal channels of the framework. Based on the change in point group symmetry of the linker

12121

dx.doi.org/10.1021/ja506230r | J. Am. Chem. Soc. 2014, 136, 12119–12129
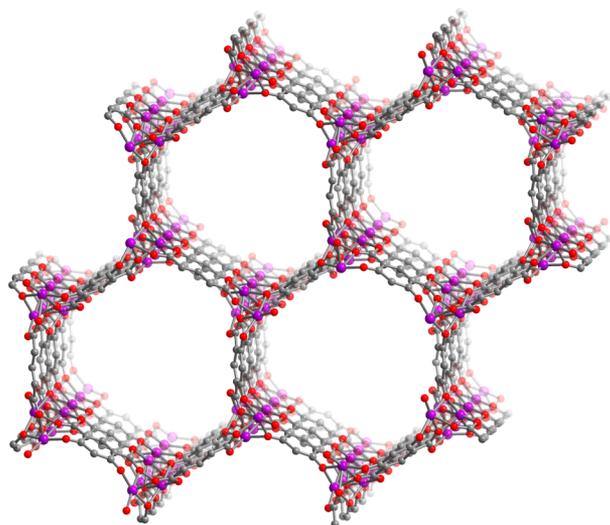
Figure 2. Crystal structure of $Co_2(m\text{-dobdc})$ showing one-dimensional hexagonal pores and helical metal chains.

from C_{2h} in $H_4(dobdc)$ to C_{2v} in $H_4(m\text{-dobdc})$, a change in the space group from $R\bar{3}$ in $Co_2(dobdc)$ to $R3m$ in $Co_2(m\text{-dobdc})$ is observed.[4a] Additional structural differences between the two compounds are apparent.[9e] For instance, the orientation of the carboxylate groups of the linker is changed, with the CO_2^- unit twisting out of the plane of the aromatic ring by approximately 12.5° in $Co_2(m\text{-dobdc})$, as compared to just 3.5° in $Co_2(dobdc)$. Furthermore, metal centers in $Co_2(m\text{-dobdc})$ that face into the same pore align directly along the crystallographic b axis, resulting in a Co···Co separation of 14.9(1) Å across the channels. In $Co_2(dobdc)$, the metals are offset from each other by one-third of a twist in the chain, leading to a Co···Co separation of 15.24(8) Å across the channels. A structureless Le Bail refinement of the other $M_2(m\text{-dobdc})$ (M = Mg, Mn, Fe, Ni) compounds afforded related unit cells, confirming that the entire series is isostructural.

With such similar crystal structures, the surface areas would be expected to be similar for the two types of frameworks. Indeed, a geometric approximation of the surface areas for $Co_2(m\text{-dobdc})$ and $Co_2(dobdc)$ predicts them to both be 1297 m^2/g.[23] Low-pressure N_2 adsorption isotherms collected at 77 K reveal type I isotherms characteristic of microporous solids for the $M_2(m\text{-dobdc})$ (M = Mn, Fe, Co, Ni) compounds (Figure S11). Langmuir and BET surface areas were calculated (Table 1), and in each case the results are comparable to those reported for $M_2(dobdc)$.[4b,c,9e,24] Based on the similar framework structure, this indicates full evacuation of the pores and complete desolvation of the framework. Furthermore, the $Co_2(m\text{-dobdc})$ BET surface area of 1264 m^2/g is very close to the predicted surface area of 1297 m^2/g from the geometric calculations. Achieving complete activation of the Mg analogue

has proven challenging, and all efforts have thus far resulted in materials with lower than expected surface areas. As a result, the remaining data will focus only on the other four $M_2(m\text{-dobdc})$ compounds.

H_2 Adsorption Isotherms. To probe the potentially modified electronic structures at the open metal coordination sites, low-pressure H_2 adsorption isotherms were measured for the four $M_2(m\text{-dobdc})$ (M = Mn, Fe, Co, Ni) frameworks at 77 and 87 K (Figures S20−S23). As for the $M_2(dobdc)$ series,[4a] $Ni_2(m\text{-dobdc})$ has the greatest H_2 uptake at 77 K and 1 bar, followed by Fe, Mn, and Co compounds, respectively. Although the $M_2(dobdc)$ frameworks have a higher H_2 uptake at 1 bar, in the very low-pressure regime, $Ni_2(m\text{-dobdc})$ has a significantly higher uptake than $Ni_2(dobdc)$ at both 77 and 87 K (Figure S27). This indicates that the interaction of H_2 with the exposed Ni^{2+} cations ion the surface of $Ni_2(m\text{-dobdc})$ is stronger than in $Ni_2(dobdc)$; since these frameworks have about the same surface area, another effect must be influencing the binding strength of H_2.

Isosteric heats of H_2 adsorption were calculated in order to gain insight into this increased low-pressure H_2 adsorption and confirm whether there is indeed a stronger interaction between H_2 and the metal centers in the $M_2(m\text{-dobdc})$ frameworks. In order to determine the isosteric heat of adsorption (Q_{st}) using the Clausius−Clapeyron relation, H_2 isotherm data at 77 and 87 K were fit with either a dual-site Langmuir−Freundlich equation or a trisite Langmuir equation. Similar to $M_2(dobdc)$,[4a] the isosteric heat of adsorption plots for $M_2(m\text{-dobdc})$ imply a nearly constant H_2 binding enthalpy until a loading of 0.7−0.8 H_2/M^{2+}, followed by a sharp decrease as all exposed metal cations become occupied and only weaker adsorption sites are available (Figure 3). The inflection points
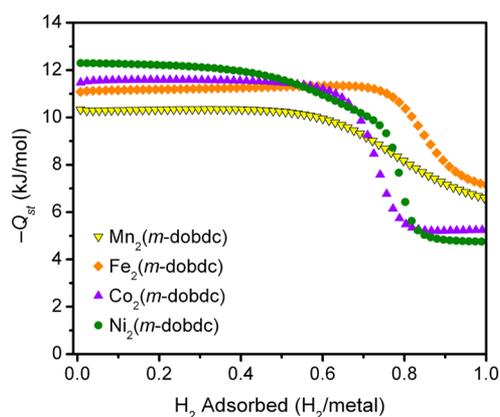
Figure 3. H_2 isosteric heat of adsorption curves for the $M_2(m\text{-dobdc})$ series of frameworks, as a function of the amount adsorbed.

range from ∼0.75 H_2/M in $Co_2(m\text{-dobdc})$ to ∼0.85 H_2/M in $Fe_2(m\text{-dobdc})$, which corresponds with the fraction of metal sites available for H_2 binding. These values are comparable to previously observed values for the $M_2(dobdc)$ series.[24]

Increasing the binding enthalpy of H_2 in metal−organic frameworks is important for practical applications, as a binding enthalpy of −15 to −20 kJ/mol is predicted to be optimal for the on-board storage of H_2 at ambient temperatures.[25] The low-coverage isosteric heats of adsorption of $Mn_2(m\text{-dobdc})$, $Fe_2(m\text{-dobdc})$, $Co_2(m\text{-dobdc})$, and $Ni_2(m\text{-dobdc})$ are −10.3, −11.1, −11.6, and −12.3 kJ/mol, respectively. This trend in binding enthalpies for H_2 is consistent with the Irving−

Table 1. Langmuir and BET Surface Areas of the $M_2(dobdc)$ and $M_2(m\text{-dobdc})$ Frameworks[a]

		Mn[4b,9e]	Fe[4c]	Co[24a]	Ni[24b]
$M_2(dobdc)$	Langmuir (m^2/g)	1797	1535	1432	1574
	BET (m^2/g)	1102	1360	1341	
$M_2(m\text{-dobdc})$	Langmuir (m^2/g)	1741	1624	1504	1592
	BET (m^2/g)	1349	1295	1264	1321

[a]The values for $M_2(dobdc)$ are from literature sources.

Williams series, which predicts that high-spin complexes increase in stability moving from Groups 7 to 10.[26] The trend further mirrors that observed for H_2 binding within M_2(dobdc) frameworks (Table 2). Calculated isosteric heat of

Table 2. Comparison of Low-Loading H_2 Isosteric Heats of Adsorption (Q_{st}, kJ/mol) in M_2(dobdc) and M_2(m-dobdc)[a]

|	Mn	Fe	Co	Ni
M_2(dobdc)	−8.8	−9.7	−10.8	−11.9
M_2(m-dobdc)	−10.3	−11.1	−11.5	−12.3

[a]The M_2(dobdc) values are from this work to make an accurate comparison except for Fe_2(dobdc), which was previously reported by our group and fit in the same manner.[4c] Other literature values are also available.[4a]

adsorption values are highly sensitive to the fitting equation used, the temperatures at which data are collected and the quality of the fits. Given this, the values for the M_2(dobdc) series were calculated from isotherms collected in this work (except Fe_2(dobdc), which was previously reported by our group and fit using the same method)[4c] in order to maintain consistency in the collected isotherms and the manner in which they are fit. These values all agree with the literature values for the M_2(dobdc) series except for Ni_2(dobdc), which we found to be 1 kJ/mol less than the literature value of −12.9 kJ/mol.[4a] This discrepancy most likely arises from a difference in data collection, isotherm temperatures, and equation used to fit the data. Consequently, our data that were collected and fit in the same manner as the M_2(m-dobdc) data presented here are used for comparison. Importantly, the isosteric heats of adsorption for the M_2(m-dobdc) compounds are, on average, ∼1.0 kJ/mol stronger than in the corresponding M_2(dobdc) frameworks

(Table 2) and are as much as 1.5 kJ/mol stronger in the case of Mn, which also has the largest percent increase (17%) in binding enthalpy.

Powder Neutron Diffraction. In an effort to understand further why the M_2(m-dobdc) frameworks show higher H_2 binding enthalpies than the structurally similar M_2(dobdc), neutron diffraction experiments were performed on microcrystalline powder samples dosed with precise quantities of D_2. Data were collected upon successively dosing the evacuated Co_2(m-dobdc) and Ni_2(m-dobdc) samples with loadings ranging from 0.75 to 3.0 D_2 molecules per metal center and cooling to 10 K. Based on previous results for M_2(dobdc) frameworks[6c] as well as the isosteric heats of adsorption for M_2(m-dobdc) that begin to decrease at loadings near 1 H_2/metal, it was anticipated that the open metal coordination site would provide the primary hydrogen binding site. Indeed, this site, designated site I, was found to be the only D_2 binding site in Co_2(m-dobdc) at the lowest loading of 0.75 D_2 per Co^{2+} (Figure 4a). The center of the D_2 electron density was observed to be at a separation of 2.23(5) Å from the metal center, closer than the 2.32(2) Å found for Co_2(dobdc) at the same loading (Tables S12−S13), which is further confirmation that the hydrogen binds more strongly to the open metal sites within the *meta* framework. The same binding site is apparent in Ni_2(m-dobdc), with a comparable M···D_2 distance of 2.18(4) Å at a loading of 1.0 D_2 per Ni^{2+}, which is within error of the distance of 2.201(1) Å observed for Ni_2(dobdc) at 4 K.[27]

Increasing the D_2 loading in Co_2(m-dobdc) revealed several secondary binding sites. At a loading of 1.25 D_2 per metal, a second binding site (site II) adjacent to the primary site becomes populated (Figure 4b). This can be attributed to a D_2···D_2 interaction based on a short D_2···D_2 separation of 2.88(4) Å, combined with a D_2···O interaction occurring at a
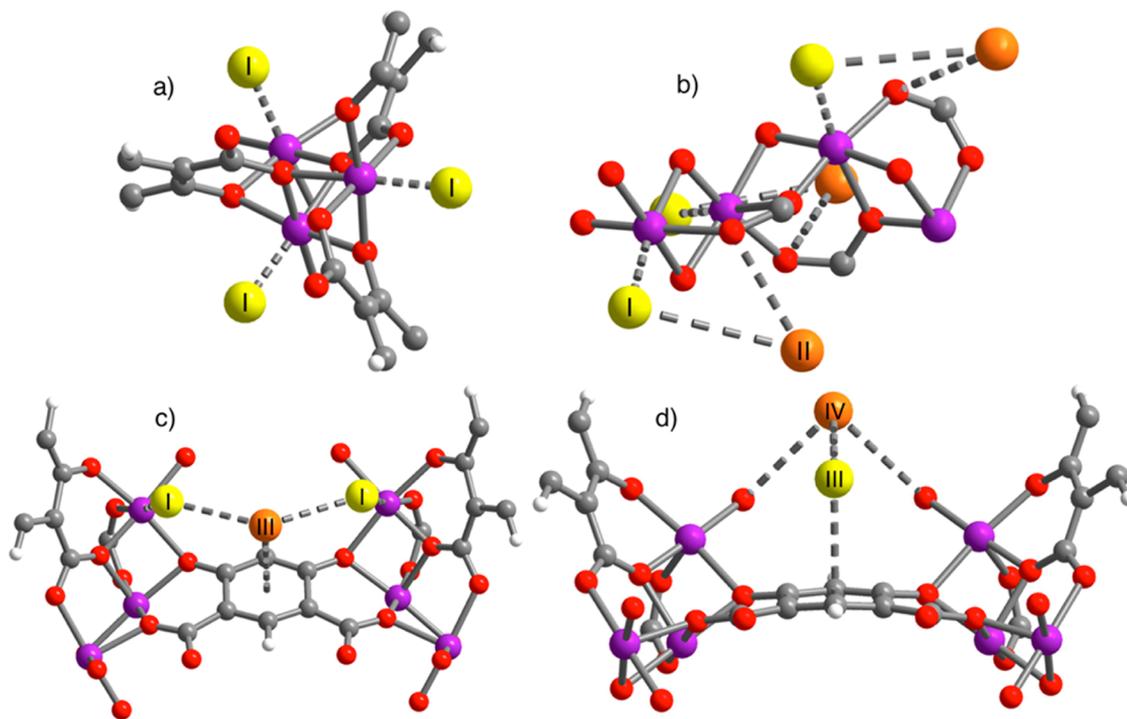
Figure 4. Partial crystal structures at 10 K of Co_2(m-dobdc) showing (a) the primary binding site (site I) on the open metal site; (b) binding site II interacting with the D_2 in site I; (c) binding site III on the aromatic ring in the linker; and (d) binding site IV, interacting with the D_2 in site III. Purple, gray, red, and white spheres represent Co, C, O, and H atoms, respectively. Yellow and orange spheres represent D_2 molecules.

separation of 3.28(6) Å from the nearest framework oxygen atom. Site II is in a similar location to the secondary binding sites observed in $Co_2(dobdc)$ and $Mg_2(dobdc)$,[6c] whereby the second bound D_2 appears to rely on $D_2\cdots D_2$ interactions in all cases. The site I to site II $D_2\cdots D_2$ separation, however, of 3.05(2) Å in $Co_2(m\text{-dobdc})$ at a loading of 2.25 D_2 per metal is significantly shorter than the 3.16(2) Å observed at the same loading in $Co_2(dobdc)$ or the 3.16(8) Å arising for a similar loading of 1.2 D_2 per metal in $Mg_2(dobdc)$. This closer site I to site II separation in $Co_2(m\text{-dobdc})$ is most likely a polarization effect, as the more strongly bound D_2 residing at site I has a larger induced dipole, leading to a stronger interaction with a D_2 molecule adsorbed at site II.

A third binding site (site III) located approximately 3.08 Å above the mean plane of the aromatic ring of the $m\text{-dobdc}^{4-}$ linker becomes populated at higher loadings of D_2. This site is equidistant (3.25(6) Å) to two D_2 molecules at neighboring site I positions in $Co_2(m\text{-dobdc})$, whereas in $Co_2(dobdc)$, the different symmetry leads to two distinct site I$\cdots$site III interactions at distances of 3.06(3) and 3.24(3) Å. Importantly, for $Co_2(m\text{-dobdc})$ there are only half as many D_2 molecules situated at site III as in $Co_2(dobdc)$ at high loadings, which leads to the observation of a fourth binding site (site IV) not seen in the $M_2(dobdc)$ series. We note that a fourth site was identified in $Zn_2(dobdc)$,[6b] but this is not the same site seen in the $Co_2(m\text{-dobdc})$ case. The differing symmetry of the *meta* framework contributes to this additional binding site, as the two framework oxygen atoms interacting with the D_2 molecule in site IV are equivalent in $Co_2(m\text{-dobdc})$, but not in $Co_2(dobdc)$. Relative to site I, larger atomic displacement parameters for the refined D_2 molecules at binding sites II, III, and IV are also indicative of weaker interactions. Neutron diffraction measurements of $Ni_2(m\text{-dobdc})$ with different loadings of D_2 resulted in the identification of the same binding sites as those found for $Co_2(m\text{-dobdc})$ (Tables S21−S23).

Neutron diffraction experiments intended to elucidate binding sites are generally performed using D_2 instead of H_2 because the large incoherent scattering cross-section of H atoms contributes strongly to the background and reduces data quality. In addition, the coherent scattering cross-section of a D atom is approximately four times larger than that of an H atom. While it has been shown through gas adsorption measurements that metal−organic frameworks tend to adsorb D_2 slightly more strongly than H_2,[28] it has been assumed that both molecules behave similarly when binding, only displaying extremely minor differences in interaction distances. In order to test this assumption, we measured and successfully refined the structure of $Co_2(m\text{-dobdc})$ dosed with a low loading of H_2. We believe this is the first structural data from powder neutron diffraction reported for H_2 in a metal−organic framework. As expected from the D_2 data, a dose below 1.0 H_2 per metal site resulted in binding exclusively at site I. Interestingly, the center of the H_2 density was found to be 2.26(4) Å from the Co atom, perhaps slightly longer than the $Co\cdots D_2$ distance of 2.23(5) Å, although still within the associated error. Whether this is indicative of a slightly stronger interaction with D_2 is somewhat unclear due to the resolution of the data; however, it does confirm that H_2 and D_2 can be expected to behave similarly for the purposes of structural determination.

Inelastic Neutron Scattering. Inelastic neutron scattering (INS) experiments were carried out to probe the site-specific binding properties of H_2. Data for various loadings of H_2 after subtraction of the spectra for the evacuated materials are shown

in Figure 5. At loadings up to and including 1.0 $n\text{-}H_2$ (corresponding to a 3:1 *ortho*-H_2:*para*-H_2 ratio) molecule per
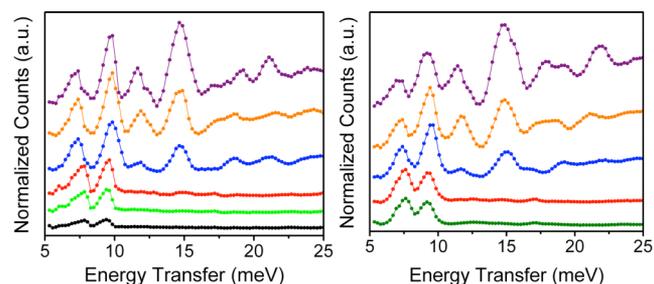
Figure 5. INS data for $Co_2(m\text{-dobdc})$ (left) and $Ni_2(m\text{-dobdc})$ (right) at loadings of 0.33 (black), 0.50 (dark green), 0.67 (light green), 1.0 (red), 2.0 (blue), 3.0 (yellow), and 4.0 (purple) $n\text{-}H_2$ molecules per metal atom. Data are shown after subtraction of the spectrum of the evacuated framework and offset for clarity.

metal atom, two low-energy rotational lines are apparent at 7.8(1) and 9.5(1) meV for $Co_2(m\text{-dobdc})$ and 7.5(1) and 9.3(1) meV for $Ni_2(m\text{-dobdc})$. These features are similar to those observed in INS spectra for several compounds in the $M_2(dobdc)$ series at low loadings and have been assigned to transitions occurring from the $J = 0$ state to sublevels of the split $J = 1$ rotational state for initial H_2 molecules adsorbed at the metal centers.[4c,6b,c,24] This assignment has been confirmed through correlation with neutron diffraction and DFT calculations.[29] Presumably, there is also a higher-energy transition, not collected within this current data range, as seen in the $M_2(dobdc)$ series. The splitting between the low-energy peaks of approximately 1.6 meV for both $Co_2(m\text{-dobdc})$ and $Ni_2(m\text{-dobdc})$ is smaller than that observed for any of the $M_2(dobdc)$ materials. The position of the first peak is at higher energies than that of the first peak of the $M_2(dobdc)$ frameworks (except for the Zn analogue), and the position of the second peak is at lower energies than is observed for all the $M_2(dobdc)$ compounds. The energy splitting of these peaks has been previously shown to have no correlation with the binding strength of H_2 at the open metal site.[30]

At loadings above 0.75 H_2 molecules per metal, as sites II−IV begin to populate, the additional H_2 molecules affect the rotational potential for H_2 molecules at site I. This adjusts the rotational energy level, resulting in a shift of the first peak to lower energies and the second peak to higher energies. These peak shifts are similar to those observed for the $M_2(dobdc)$ frameworks, with magnitudes of approximately 0.7 meV for $Co_2(m\text{-dobdc})$ and 0.5 meV for $Ni_2(m\text{-dobdc})$, though much less than the 1.4 meV shift observed for $Fe_2(dobdc)$.[4c] Adsorption of H_2 at the secondary sites also results in a significant increase in the area of the peak at 9 meV and appearance of features near 12 and 15 meV as a new subset of rotational levels associated with the rotationally hindered second adsorption site. Transitions in this energy range are also observed in spectra reported for higher loadings of the $M_2(dobdc)$ materials, indicating the similarity in adsorption potentials at these secondary sites.[4c,6c]

Infrared Spectra. Since the higher binding enthalpies and low-coverage H_2 uptake cannot reasonably be attributed to a significant change in the macrostructure of the framework, infrared spectroscopy was used to further probe the binding of H_2 at the open metal coordination sites. The vibrational frequency of adsorbed H_2 is almost always lower than that of

the molecule in the gas phase (4161 cm^{-1}), and it is now well established that for metal−organic frameworks, there is a strong correlation between the magnitude of the frequency shift and the binding energy at a particular site.[31] A comparison of the H$_2$ vibrational frequencies is shown at two different H$_2$ loadings for Ni$_2$(m-dobdc), Ni$_2$(dobdc), Co$_2$(m-dobdc), and Co$_2$(dobdc) (Figure 6) and for Mn$_2$(m-dobdc) and Mn$_2$(dobdc) (Figure
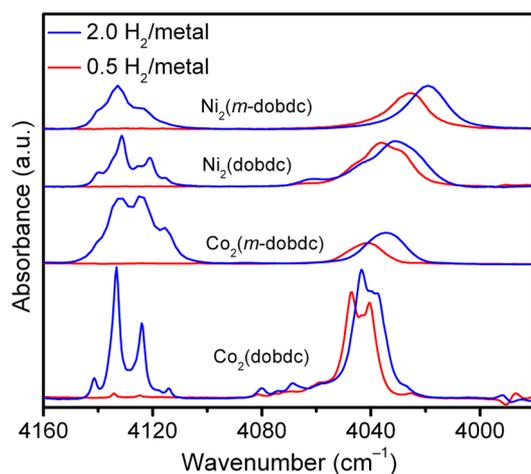
Figure 6. Comparison of the IR spectra of Ni$_2$(m-dobdc), Ni$_2$(dobdc), Co$_2$(m-dobdc), and Co$_2$(dobdc) at two different concentrations. The right peak shows the H$_2$ bound to the open metal site, and the left peak shows the H$_2$ bound to the secondary adsorption sites. Spectra are offset for clarity.

S45). At this temperature, the pure vibrational part of the spectrum consists of an ortho−para pair that is separated by just 6 cm^{-1} in the gas phase. The peak near 4025 cm^{-1} in each spectrum corresponds to the H$_2$ bound to the open metal site.

In each case, the spectra for loadings of 0.5 H$_2$ molecules per metal, which are known to arise purely from H$_2$ bound to the open metal site, show a greater frequency shift for the Co$_2$(m-dobdc) and Ni$_2$(m-dobdc) than for Co$_2$(dobdc) or Ni$_2$(dobdc). This shift is consistent with the stronger H$_2$ binding observed in the M$_2$(m-dobdc) frameworks based on equilibrium adsorption isotherms and neutron diffraction studies. Upon further loading, the secondary adsorption sites begin to be populated, which is evidenced by a second peak that grows in around 4125 cm^{-1}. The energy of the peaks associated with the secondary sites is very similar to those seen for M$_2$(dobdc), consistent with the INS transitions for H$_2$ bound to the secondary sites, which were also similar between M$_2$(m-dobdc) and M$_2$(dobdc) compounds. This supports our hypothesis that the electronic structure at the metal center is significantly altered with the m-dobdc$^{4−}$ linker, leading to a higher initial isosteric heat of adsorption, while the secondary sites in M$_2$(m-dobdc) and M$_2$(dobdc) are similar in binding potential due to structural similarities between the two frameworks. Furthermore, a consistent shift in the frequency for the metal-adsorbed H$_2$ molecules as a function of concentration is seen for both the Co$_2$(m-dobdc) and Ni$_2$(m-dobdc) samples, although not to the same degree in the Mn$_2$(m-dobdc) sample. These concentration shifts have previously been attributed to H$_2\cdots$H$_2$ interactions, and it is interesting to note that the shifts seem largely unaffected by the change in linker. Furthermore, these shifts correlate well with the shifts seen in rotational potential as the secondary binding sites are populated in the INS data shown in Figure 5.

Variable-temperature infrared spectroscopy is a standard technique for establishing the enthalpy of adsorption at a particular site.[32] Figure 7 shows the spectra obtained for H$_2$ in
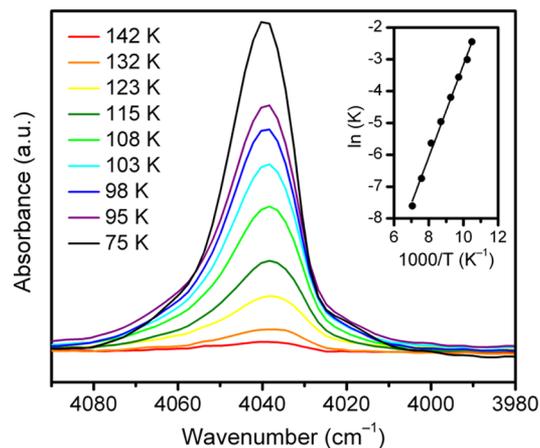
Figure 7. Variable-temperature infrared spectra of Co$_2$(m-dobdc). The inset shows the van't Hoff plot that is used to extract the enthalpy and entropy change in H$_2$ upon adsorption to the open metal site.

Co$_2$(m-dobdc) while lowering the sample temperature from 142 to 75 K. In each case, the initial H$_2$ pressure for the system was set such that only the open metal site was occupied over the full temperature range. The fractional occupancy is then determined by the ratio of the area under the infrared band to that observed at complete saturation. The inset in Figure 7 shows the van't Hoff relationship plot used to extract both the enthalpy and entropy change upon adsorption. The data obtained in this way for the different materials are summarized in Table 3. The slopes extracted from the van't Hoff plots are

Table 3. Enthalpy and Entropy Changes upon Adsorption of H$_2$ to the Open Metal Site[a]

	M$_2$(dobdc)		M$_2$(m-dobdc)	
M	ΔS (J/mol K)	ΔH (kJ/mol)	ΔS (J/mol K)	ΔH (kJ/mol)
Mn	—	—	−135	−10.5
Co	−136	−10.7	−147	−12.1
Ni	−148	−12.3	−147	−13.7

[a]Values are extracted from a van't Hoff plot based on the area of the infrared vibrational peaks for a given temperature and pressure.

sensitive to small variations in the maximum saturation area; as such, an error on the order of 0.5 kJ/mol is estimated. Even with these limitations, the data is consistent with the calculated isosteric heats of adsorption from the H$_2$ adsorption isotherms, showing an enthalpy increase from Mn to Co to Ni. More importantly, these infrared spectroscopy-based heat of adsorption values are about 1.4 kJ/mol larger than those calculated for their respective M$_2$(dobdc) counterparts from similar infrared experiments. The binding enthalpy of −13.7 kJ/mol in Ni$_2$(m-dobdc) is among the highest reported H$_2$ binding enthalpies in a metal−organic framework to date. This is consistent with the trends observed using values calculated from H$_2$ adsorption isotherms. We further note that the measured large entropy changes are consistent with previous studies, in which a strong correlation between the enthalpy and entropy change of the bound hydrogen in different metal−organic frameworks was observed.[33] Overall, the redshift seen

in the infrared spectra for the adsorbed H_2 in $M_2(m\text{-dobdc})$ as compared to $M_2(\text{dobdc})$ indicates that the H_2 is more strongly bound, and the variable-temperature data confirms the increased binding enthalpies seen from the H_2 adsorption data.

Electronic Structure Calculations. Density functional theory (DFT) was used to examine the differences in the electronic structures at the open metal sites by using representative complexes to model the $M_2(\text{dobdc})$ and $M_2(m\text{-dobdc})$ frameworks. DFT has shown itself to be a fairly robust method for modeling chemical systems; its major failings, self-interaction error and lack of dispersion interactions,[34] are well-known and can be corrected for by using appropriate functionals that account for these failings, namely range separation and explicit dispersion correction.[35] Previously, the ωB97X-D[36] functional was shown to accurately model H_2 binding in metal−organic frameworks.[37]

Modeling $M_2(\text{dobdc})$-type frameworks accurately with electronic structure theory is challenging because fragmenting the structure at any point will lead to the neglect of important interactions from the chains formed by the M^{2+} ions. In an attempt to understand the nature of the differences in hydrogen binding between $M_2(\text{dobdc})$ and $M_2(m\text{-dobdc})$, some accuracy in the calculated energetics is sacrificed in order to learn relevant information about the differences between the two systems. In this vein, our modeling focused on the linker of interest coordinated to two Co^{2+} centers; the remaining ligands on each Co^{2+} ion were truncated as formaldehyde molecules in order to maintain charge balance. Since the key open coordination site for each Co^{2+} center in the framework is enforced by constraints on the ligands imposed by the macrostructure of the framework, which could not be explicitly included in our model, an unconstrained optimized geometry of the model would not actually reflect the structural properties of the framework in question. Thus, the geometry of the linker complex was taken from the experimentally determined crystal structure of the framework and subsequently frozen before the interaction with H_2 was optimized. Furthermore, the $Co\cdots H_2$ distance was taken from the neutron diffraction spectra and used as a constraint to ensure an accurate depiction of this interaction in the model system.

While comparing absolute energy differences gives a single number to describe H_2 binding, energy decomposition analysis (EDA) breaks down that number into physically interpretable components. An EDA based on absolutely localized molecular orbitals (ALMOs)[21] breaks down total binding energies into frozen energy, polarization, and charge-transfer components. The frozen term is due to permanent electrostatics and Pauli repulsions, since the H_2 electron density is being brought within the van der Waals radius of the Co atom. The polarization term corresponds to the favorable interaction of electrons in the H_2 and complex fragments relaxing in the presence of the other fragment without electron transfer. Charge transfer stems from energy lowering when electrons are allowed to flow from one fragment to the other. A recent generalization of the ALMO EDA to open-shell molecules allows for the application of this method to general metal-containing systems.[38]

The binding energy decomposition analysis clarifies the differences in these two species (Table 4). Specifically, there is more charge transfer and polarization in the $m\text{-dobdc}^{4-}$-containing complex, which is accompanied by a partially offsetting increase in the energetically unfavorable frozen term. This larger frozen term is the result of the increased steric

Table 4. ALMO Energy Decomposition Analysis of H_2 Binding to the dobdc^{4-} and $m\text{-dobdc}^{4-}$ Complexes

	energy (kJ/mol)	
component	dobdc^{4-}	$m\text{-dobdc}^{4-}$
frozen	1.3	7.9
polarization	−4.8	−9.5
charge transfer	−12.5	−17.1
total	−16.0	−18.6

repulsion that stems from a shorter $Co\cdots H_2$ distance in the $m\text{-dobdc}^{4-}$ complex. The increased charge-transfer energy of H_2 binding in this species is key, as that is the largest term in the total calculated binding energy. A breakdown of the charge-transfer term can be seen in Table 5; in both cases, the largest

Table 5. Forward and Backbonding Contributions to the Charge-Transfer Term for the dobdc^{4-} and $m\text{-dobdc}^{4-}$ Complexes

	energy (kJ/mol)	
	dobdc^{4-}	$m\text{-dobdc}^{4-}$
$H_2 \rightarrow Co$ bonding	−9.1	−11.8
$Co \rightarrow H_2$ backbonding	−3.4	−5.3

portion of the charge transfer comes from the H_2 σ orbital to the unoccupied orbitals of the Co complex. The increased H_2 to Co forward donation is indicative of more positive charge at the metal cation in the $m\text{-dobdc}^{4-}$ complex as compared with the dobdc^{4-} complex. This explains the experimentally determined increase in binding enthalpy of H_2 in the $M_2(m\text{-dobdc})$ frameworks as compared with their $M_2(\text{dobdc})$ analogues, as increased positive charge at the metal center leads to stronger polarization of the bound H_2. Additionally, a difference is seen in the location of the bound H_2 relative to the linker in the two complexes. In the dobdc^{4-} linker complex, the H_2 binds to create a nearly octahedral geometry around the Co^{2+} ion, with a distance of 3.30 Å from the H_2 to the aromatic carbon bonded to the carboxylate group (the α carbon). Conversely, in the $m\text{-dobdc}^{4-}$ complex, the H_2 is reoriented toward the linker at a distance of 2.64 Å from the α carbon (Figure 8a,b). This difference suggests that a change in the charge at the α carbon due to the different symmetry of the $m\text{-dobdc}^{4-}$ linker possibly facilitates a change in the binding geometry for H_2. While this significant change may be an artifact associated with the small cluster models, it is the same trend seen experimentally for the $H_2\cdots\alpha$ carbon distance, which is 3.48(3) Å in $Co_2(m\text{-dobdc})$ and 3.59(2) Å in $Co_2(\text{dobdc})$.

The orbital interactions between H_2 and the Co complexes provide further insight into the stronger H_2 binding in $Co_2(m\text{-dobdc})$. While increased forward bonding is a product of increased charge density at the metal, the nature of the backbonding from the complex to H_2 is quite different. This can be seen by looking at the complementary occupied virtual orbital pairs (COVPs) that contribute most to backbonding (Figure 8c,d). In the dobdc^{4-} complex, the occupied orbital is primarily localized on the metal center, while in the $m\text{-dobdc}^{4-}$ species, the donating orbital includes contributions from the π system of the linker. This increased backbonding for $m\text{-dobdc}^{4-}$ agrees with the redshift seen in the H_2 infrared spectra for the $M_2(m\text{-dobdc})$ frameworks, as increased backbonding will weaken the H−H bond. This possible extra interaction with the linker in the $m\text{-dobdc}^{4-}$ complex, coupled with the larger
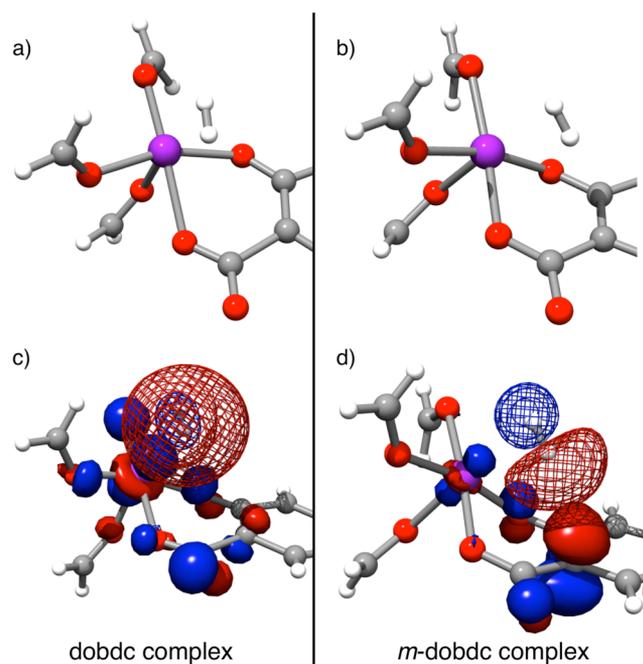
Figure 8. Calculated binding modes of H$_2$ in (a) the dobdc complex and (b) the *m*-dobdc complex, in both of which the Co^{2+} is purple and the H$_2$ is above the Co^{2+}. The corresponding COVPs are shown for (c) the dobdc complex and (d) the *m*-dobdc complex, with occupied and virtual orbitals shown as solid and mesh, respectively, at a 0.05 Å$^{-3/2}$ isodensity.

forward donation of the H$_2$ to the more positively charged metal center, are the key differences between these two systems that help to explain the stronger H$_2$ binding seen in M$_2$(*m*-dobdc) versus M$_2$(dobdc).

CONCLUSIONS

The foregoing results demonstrate the synthesis of a new family of metal—organic frameworks, M$_2$(*m*-dobdc) (M = Mg, Mn, Fe, Co, Ni), representing a potentially less expensive version of their well-known structural isomers M$_2$(dobdc). Hydrogen was used as an initial probe to determine how electronic and structural differences in the new frameworks modified the interactions of the open metal coordination sites with adsorbates. The Mn, Fe, Co, and Ni variants exhibited greater isosteric heats of H$_2$ adsorption by approximately 1 kJ/mol compared to the M$_2$(dobdc) compounds. The results from powder neutron diffraction, inelastic neutron scattering, and infrared spectroscopy experiments performed on hydrogen-loaded samples of Co$_2$(*m*-dobdc) all support this as arising from stronger interactions between the metal centers and the H$_2$ molecules. Future efforts will focus on the larger-scale production of M$_2$(*m*-dobdc) compounds and determining whether the enhanced charge density at the metal sites leads to improvements compared to their M$_2$(dobdc) analogues in the efficacy of key gas separations, including O$_2$ from air,[1j,39] CO$_2$/N$_2$,[1h,j,7a,40] CO$_2$/H$_2$,[1j,41] CO/H$_2$,[1e,39a,42] ethylene/ethane,[1i,9] propylene/propane,[1i,3d,9] and methane purification.[43]

ASSOCIATED CONTENT

S Supporting Information

Additional framework characterization, powder diffraction patterns, thermogravimetric analyses, infrared spectra, BET isotherm fits, adsorption isotherms, details on isotherm fitting,

neutron diffraction atomic parameters, Rietveld refinement plots, additional VTIR spectra, COVPs, and additional experimental details. This material is available free of charge via the Internet at http://pubs.acs.org.

AUTHOR INFORMATION

Corresponding Author
jrlong@berkeley.edu

Present Address
¶Department of Chemistry and Biochemistry, Mount Allison University, Sackville, New Brunswick, Canada E4L 1G8

Notes
The authors declare no competing financial interest.

REFERENCES

(1) (a) Eddaoudi, M.; Kim, J.; Rosi, N.; Vodak, D.; Wachter, J.; O'Keeffe, M.; Yaghi, O. M. *Science* **2002**, *295*, 469. (b) Kitagawa, S.; Kitaura, R.; Noro, S.-I. *Angew. Chem., Int. Ed.* **2004**, *43*, 2334. (c) Millward, A. R.; Yaghi, O. M. *J. Am. Chem. Soc.* **2005**, *127*, 17998. (d) Ma, S.; Sun, D.; Simmons, J. M.; Collier, C. D.; Yuan, D.; Zhou, H.-C. *J. Am. Chem. Soc.* **2008**, *130*, 1012. (e) Britt, D.; Tranchemontagne, D.; Yaghi, O. M. *Proc. Natl. Acad. Sci. U.S.A.* **2008**, *105*, 11623. (f) Li, J.-R.; Kuppler, R. J.; Zhou, H.-C. *Chem. Soc. Rev.* **2009**, *38*, 1477. (g) Britt, D.; Furukawa, H.; Wang, B.; Glover, T. G.; Yaghi, O. M. *Proc. Natl. Acad. Sci. U.S.A.* **2009**, *106*, 20637. (h) Sumida, K.; Rogow, D. L.; Mason, J. M.; McDonald, T. M.; Bloch, E. D.; Herm, Z. R.; Bae, T.-H.; Long, J. R. *Chem. Rev.* **2012**, *112*, 724. (i) Bloch, E. D.; Queen, W. L.; Krishna, K.; Zadrozny, J. M.; Brown, C. M.; Long, J. R. *Science* **2012**, *335*, 1606. (j) Li, J.-R.; Sculley, J.; Zhou, H.-C. *Chem. Rev.* **2012**, *112*, 869.

(2) (a) Suh, M. P.; Park, H. J.; Prasad, T. K.; Lim, D.-W. *Chem. Rev.* **2012**, *112*, 782. (b) Konstas, K.; Osl, T.; Yang, Y.; Batten, M.; Burke, N.; Hill, A. J.; Hill, M. R. *J. Mater. Chem.* **2012**, *22*, 16698.

(3) (a) Dincă, M.; Dailly, A.; Liu, Y.; Brown, C. M.; Neumann, D. A.; Long, J. R. *J. Am. Chem. Soc.* **2006**, *128*, 16876. (b) Dietzel, P. D. C.; Johnsen, R. E.; Blom, R.; Fjellvåg, H. *Chem.—Eur. J.* **2008**, *14*, 2389. (c) Vitillo, J. G.; Regli, L.; Chavan, S.; Ricchiardi, G.; Spoto, G.;

Dietzel, P. D. C.; Bordiga, S.; Zecchina, A. *J. Am. Chem. Soc.* **2008**, *130*, 8386. (d) Bae, Y.-S.; Lee, C. Y.; Kim, K. C.; Farha, O. K.; Nicklas, P.; Hupp, J. T.; Nguyen, S.; Snurr, R. Q. *Angew. Chem., Int. Ed.* **2012**, *51*, 1857. (e) Li, Y.-W.; Li, J.-R.; Wang, L.-F.; Zhou, B.-Y.; Chen, Q.; Bu, Z.-H. *J. Mater. Chem. A* **2013**, *1*, 495. (f) Duan, X.; Cai, J.; Yu, J.; Wu, C.; Cui, Y.; Yang, Y.; Qian, G. *Microporous Mesoporous Mater.* **2013**, *181*, 99. (g) Cai, J.; Yu, J.; Xu, H.; He, Y.; Duan, X.; Cui, Y.; Wu, C.; Chen, B.; Qian, G. *Cryst. Growth Des.* **2013**, *13*, 2094.

(4) (a) Zhou, W.; Wu, H.; Yildirim, T. *J. Am. Chem. Soc.* **2008**, *130*, 15268. (b) Wu, H.; Zhou, W.; Yildirim, R. *J. Am. Chem. Soc.* **2009**, *131*, 4995. (c) Queen, W. L.; Bloch, E. D.; Brown, C. M.; Hudson, M. R.; Mason, J. A.; Murray, L. J.; Ramirez-Cuesta, A. J.; Peterson, V. K.; Long, J. R. *Dalton Trans.* **2012**, *41*, 4180.

(5) Rosi, N. L.; Kim, J.; Eddaoudi, M.; Chen, B.; O'Keeffe, M.; Yaghi, O. M. *J. Am. Chem. Soc.* **2005**, *127*, 1504.

(6) (a) Dietzel, P. D. C.; Panella, B.; Hirscher, M.; Blom, R.; Fjellvåg, H. *Chem. Commun.* **2006**, 959. (b) Liu, Y.; Kabbour, H.; Brown, C. M.; Neumann, D. A.; Ahn, C. C. *Langmuir* **2008**, *24*, 4772. (c) Sumida, K.; Brown, C. M.; Herm, Z. R.; Chavan, S.; Bordiga, S.; Long, J. R. *Chem. Commun.* **2011**, *47*, 1157.

(7) (a) Dietzel, P. D. C.; Besikiotis, V.; Blom, R. *J. Mater. Chem.* **2009**, *19*, 7362. (b) Makal, T. A.; Li, J.-R.; Lu, W.; Zhou, H.-C. *Chem. Soc. Rev.* **2012**, *41*, 7761. (c) Peng, Y.; Krungleviciute, V.; Eryazici, I.; Hupp, J. T.; Farha, O. K.; Yildirim, T. *J. Am. Chem. Soc.* **2013**, *135*, 11887.

(8) (a) Dietzel, P. D. C.; Johnsen, R. E.; Fjellvåg, H.; Bordiga, S.; Groppo, E.; Chavan, S.; Blom, R. *Chem. Commun.* **2008**, 5125. (b) Caskey, S. R.; Wong-Foy, A. G.; Matzger, A. J. *J. Am. Chem. Soc.* **2008**, *130*, 10870. (c) McDonald, T. M.; Lee, W. R.; Mason, J. A.; Wiers, B. M.; Hong, C. S.; Long, J. R. *J. Am. Chem. Soc.* **2012**, *134*, 7056. (d) Yu, D.; Yazaydin, A. O.; Lane, J. R.; Dietzel, P. D. C.; Snurr, R. Q. *Chem. Sci.* **2013**, 3544.

(9) (a) Bao, Z.; Alnemrat, S.; Yu, L.; Vasiliev, I.; Ren, Q.; Lu, X.; Deng, S. *Langmuir* **2011**, *27*, 13554. (b) He, Y.; Krishna, R.; Chen, B. *Energy Environ. Sci.* **2012**, *5*, 9107. (c) He, Y.; Zhou, W.; Krishna, R.; Chen, B. *Chem. Commun.* **2012**, *48*, 11813. (d) Wu, H.; Gong, Q.; Olson, D. H.; Li, J. *Chem. Rev.* **2012**, *112*, 836. (e) Geier, S. J.; Mason, J. A.; Bloch, E. D.; Queen, W. L.; Hudson, M. R.; Brown, C. M.; Long, J. R. *Chem. Sci.* **2013**, *4*, 2054. (f) Herm, Z. R.; Bloch, E. D.; Long, J. R. *Chem. Mater.* **2014**, *26*, 323.

(10) (a) Liu, J.; Wang, Y.; Benin, A. I.; Jakubczak, P.; Willis, R. R.; LeVan, M. D. *Langmuir* **2010**, *26*, 14301. (b) Liu, J.; Benin, A. I.; Furtado, A. M. B.; Jakubczak, P.; Willis, R. R.; LeVan, M. D. *Langmuir* **2011**, *27*, 11451.

(11) Makal, T. A.; Yakovenko, A. A.; Zhou, H.-C. *J. Phys. Chem. Lett.* **2011**, *2*, 1682.

(12) Sun, L.; Miyaki, T.; Seki, S.; Dincă, M. *J. Am. Chem. Soc.* **2013**, *135*, 8185.

(13) (a) Schlapbach, L.; Züetl, A. *Nature* **2001**, *414*, 353. (b) Collins, D. J.; Zhou, H.-C. *J. Mater. Chem.* **2007**, *17*, 3154. (c) van den Berg, A. W. C.; Areán, C. O. *Chem. Commun.* **2008**, 668. (d) Murray, L. J.; Dincă, M.; Long, J. R. *Chem. Soc. Rev.* **2009**, *38*, 1294.

(14) Lei, G.-D.; Li, L.-X.; Yu, Z. Y.; Xie, M. G. *Chin. Chem. Lett.* **2005**, *16*, 1039.

(15) Udovic, T. J.; Brown, C. M.; Leao, J. B.; Brand, P. C.; Jiggets, R. D.; Zeitoun, R.; Pierce, T. A.; Peral, I.; Copley, J. R. D.; Huang, Q.; Neumann, D. A.; Fields, R. J. *Nucl. Inst. Methods Phys. Res., Sect. A* **2008**, *588*, 406.

(16) Azuah, R. T.; Kneller, L. R.; Qiu, Y.; Tregenna-Piggott, P. L. W.; Brown, C. M.; Copley, J. R. D.; Dimeo, R. M. *J. Res. Natl. Inst. Stand. Technol.* **2009**, *114*, 241.

(17) FitzGerald, S. A.; Churchill, H. O. H.; Korngut, P. M.; Simmons, C. B.; Strangas, Y. E. *Rev. Sci. Instrum.* **2006**, *77*, 093110.

(18) Shao, Y.; Fusti Molnar, L.; Jung, Y.; Kussmann, J.; Ochsenfeld, C.; Brown, S. T.; Gilbert, A. T. B.; Slipchenko, L. V.; Levchenko, S. V.; O'Neill, D. P.; DiStasio, R. A., Jr.; Lochan, R. C.; Wang, T.; Beran, G. J. O.; Besley, N. A.; Herbert, J. M.; Lin, C. Y.; Van Voorhis, T.; Chien, S. H.; Sodt, A.; Steele, R. P.; Rassolov, V. A.; Maslen, P. E.; Korambath, P. P.; Adamson, R. D.; Austin, B.; Baker, J.; Byrd, E. F. C.; Dachsel, H.;

Doerksen, R. J.; Dreuw, A.; Dunietz, B. D.; Dutoi, A. D.; Furlani, T. R.; Gwaltney, S. R.; Heyden, A.; Hirata, S.; Hsu, C.-P.; Kedziora, G.; Khalliulin, R. Z.; Klunzinger, P.; Lee, A. M.; Lee, M. S.; Liang, W. Z.; Lotan, I.; Nair, N.; Peters, B.; Proynov, E. I.; Pieniazek, P. A.; Rhee, Y. M.; Ritchie, J.; Rosta, E.; Sherrill, C. D.; Simmonett, A. C.; Subotnik, J. E.; Woodcock, H. L., III; Zhang, W.; Bell, A. T.; Chakraborty, A. K.; Chipman, D. M.; Keil, F. J.; Warshel, A.; Hehre, W. J.; Schaefer, H. F., III; Kong, J.; Krylov, A. I.; Gill, P. M. W.; Head-Gordon, M. *Phys. Chem. Chem. Phys.* **2006**, *8*, 3172.

(19) (a) Krishnan, R.; Binkley, J. S.; Seeger, R.; Pople, J. A. *J. Chem. Phys.* **1980**, *72*, 650. (b) McLean, A. D.; Chandler, G. S. *J. Chem. Phys.* **1980**, *72*, 5639.

(20) Dolg, M.; Wedig, U.; Stoll, H.; Preuss, H. *J. Chem. Phys.* **1987**, *86*, 2123.

(21) Khaliullin, R. Z.; Cobar, E. A.; Lochan, R. C.; Bell, A. T.; Head-Gordon, M. *J. Phys. Chem. A* **2007**, *111*, 8753.

(22) Khaliullin, R. Z.; Bell, A. T.; Head-Gordon, M. *J. Chem. Phys.* **2008**, *128*, 184112.

(23) Düren, T.; Millange, F.; Férey, G.; Walton, K. S.; Snurr, R. Q. *J. Phys. Chem. C* **2007**, *111*, 15350.

(24) (a) Dietzel, P. D. C.; Georgiev, P. A.; Eckert, J.; Blom, R.; Strässle, T.; Unruh, T. *Chem. Commun.* **2010**, *46*, 4962. (b) Mason, J. A.; Veenstra, M.; Long, J. R. *Chem. Sci.* **2014**, *5*, 32.

(25) (a) Bhatia, S. K.; Myers, A. L. *Langmuir* **2006**, *22*, 1688. (b) Garrone, E.; Bonelli, B.; Otero Areán, C. *Chem. Phys. Lett.* **2008**, *456*, 68. (c) Bae, Y.-S.; Snurr, R. Q. *Microporous Mesoporous Mater.* **2010**, *132*, 300.

(26) Irving, H.; Williams, J. P. *Nature* **1948**, *162*, 746.

(27) Brown, C. M.; Ramirez-Cuesta, A. J.; Her, J.-H.; Wheatley, P. S.; Morris, R. E. *Chem. Phys.* **2013**, *427*, 3.

(28) FitzGerald, S. A.; Pierce, C. J.; Rowsell, J. L. C.; Bloch, E. D.; Mason, J. A. *J. Am. Chem. Soc.* **2013**, *135*, 9458.

(29) Kong, L.; Román-Pérez, G.; Soler, J. M.; Langreth, D. C. *Phys. Rev. Lett.* **2009**, *103*, 096103.

(30) Forster, P. M.; Eckert, J.; Heiken, B. D.; Parise, J. B.; Yoon, J. W.; Jhung, S. H.; Chang, J.-S.; Cheetham, A. K. *J. Am. Chem. Soc.* **2006**, *128*, 16846.

(31) FitzGerald, S. A.; Burkholder, B.; Friedman, M.; Hopkins, J. B.; Pierce, C. J.; Schloss, J. M.; Thompson, B.; Rowsell, J. L. C. *J. Am. Chem. Soc.* **2011**, *133*, 20310.

(32) (a) Garrone, E.; Bonelly, B.; Otero Areán, C. *Chem. Phys. Lett.* **2008**, *456*, 68. (b) Otero Areán, C.; Chavan, S.; Cabello, C. P.; Garrone, E.; Palomino, G. T. *ChemPhysChem* **2010**, *11*, 3237.

(33) Areán, C. O.; Chavan, S.; Cabello, C. P.; Garrone, E.; Palomino, G. T. *ChemPhysChem* **2010**, *11*, 3237.

(34) (a) Perdew, J. P.; Zunger, A. *Phys. Rev. B* **1981**, *23*, 5048. (b) Kristyán, S.; Pulay, P. *Chem. Phys. Lett.* **1994**, *229*, 175. (c) Dutoi, A. D.; Head-Gordon, M. *Chem. Phys. Lett.* **2006**, *422*, 230.

(35) (a) Wu, X.; Vargas, M. C.; Nayak, S.; Lotrich, V.; Scoles, G. *J. Chem. Phys.* **2001**, *115*, 8748. (b) Wu, Q.; Yang, W. *J. Chem. Phys.* **2002**, *116*, 515. (c) Chai, J.-D.; Head-Gordon, M. *J. Chem. Phys.* **2008**, *128*, 084106.

(36) Chai, J.-D.; Head-Gordon, M. *Phys. Chem. Chem. Phys.* **2008**, *10*, 6615.

(37) Sumida, K.; Stück, D.; Mino, L.; Chai, J.-D.; Bloch, E.; Zavorotynska, O.; Murray, L.; Dincă, M.; Chavan, S.; Bordiga, S.; Head-Gordon, M.; Long, J. R. *J. Am. Chem. Soc.* **2013**, *135*, 1083.

(38) Horn, P. R.; Sundstrom, E. J.; Baker, T. A.; Head-Gordon, M. *J. Chem. Phys.* **2013**, *138*, 134119.

(39) (a) Kerry, F. G. *Industrial Gas Handbook: Gas Separation and Purification*; CRC Press: Boca Raton, FL, 2007. (b) Bloch, E. D.; Murray, L. J.; Queen, W. L.; Chavan, S.; Maximoff, S. N.; Bigi, J. P.; Krishna, R.; Peterson, V. K.; Grandjean, F.; Long, G. J.; Smit, B.; Bordiga, S.; Brown, C. M.; Long, J. R. *J. Am. Chem. Soc.* **2011**, *133*, 14814.

(40) (a) Yazaydin, A. O.; Benin, A. I.; Faheem, S. A.; Jakubczak, P.; Low, J. J.; Willis, R. R.; Snurr, R. Q. *Chem. Mater.* **2009**, *21*, 1425. (b) Férey, G.; Serre, C.; Devic, T.; Maurin, G.; Jobic, H.; Llewellyn, P. L.; De Weireld, G.; Vimont, A.; Daturi, M.; Chang, J.-S. *Chem. Soc. Rev.*

2011, *40*, 550. (c) Li, J.-R.; Ma, Y.; McCarthy, M. C.; Sculley, J.; Yu, J.; Jeong, H.-K.; Balbuena, P. B.; Zhou, H.-C. *Coord. Chem. Rev.* **2011**, *255*, 1791.

(41) Herm, Z. R.; Swisher, J. A.; Smit, B.; Krishna, R.; Long, J. R. *J. Am. Chem. Soc.* **2011**, *133*, 5664.

(42) (a) McCandless, F. P. *Ind. Eng. Chem. Process Des. Dev.* **1972**, *11*, 470. (b) Miyajima, H.; Kodama, A.; Goto, M.; Hirose, T. *Adsorption* **2005**, *11*, 625. (c) Karra, J. S.; Walton, K. S. *Langmuir* **2008**, *24*, 8620.

(43) (a) Zhang, Y. F.; Musseman, I. H.; Ferraris, J. P.; Balkus, K. J. *J. Membr. Sci.* **2008**, *313*, 170. (b) Bastin, L.; Bárcia, P. S.; Hurtado, E. J.; Silva, J. A. C.; Rodrigues, A. E.; Chen, B. *J. Phys. Chem. C* **2008**, *112*, 1575. (c) Bae, Y. S.; Farha, O. K.; Spokoyny, A. M.; Mirkin, C. A.; Hupp, J. T.; Snurr, R. Q. *Chem. Commun.* **2008**, 4135. (d) Mu, B.; Li, F.; Walton, K. S. *Chem. Commun.* **2009**, 2493. (e) Lee, J. Y.; Roberts, J. M.; Farha, O. K.; Sarjeant, A. A.; Scheidt, K. A.; Hupp, J. T. *Inorg. Chem.* **2009**, *48*, 9971. (f) Couck, S.; Denayer, J. F. M.; Baron, G. V.; Rémy, T.; Gascon, J.; Kaptejin, F. *J. Am. Chem. Soc.* **2009**, *131*, 6326. (g) Lee, K.; Isley, W. C., III; Dzubak, A. L.; Verma, P.; Stoneburner, S. J.; Lin, L.-C.; Howe, J. D.; Bloch, E. D.; Reed, D. A.; Hudson, M. R.; Brown, C. M.; Long, J. R.; Neaton, J. B.; Smit, B.; Cramer, C. J.; Truhlar, D. G.; Gagliardi, L. *J. Am. Chem. Soc.* **2014**, *136*, 698.